Non-contact photoacoustic tomography and ultrasonography for biomedical imaging

Rousseau, Guy; Levesque, Daniel; Blouin, Alain; Monchalin, Jean-Pierre

Publisher's version / Version de l'éditeur:
https://doi.org/10.1117/12.906874
Photons plus ultrasound : imaging and sensing 2012, 2012-03-08

Non-contact photoacoustic tomography and ultrasonography for biomedical imaging

Guy Rousseau,* Daniel Lévesque, Alain Blouin and Jean-Pierre Monchalin
Industrial Materials Institute, National Research Council Canada,
75 de Mortagne Blvd., Boucherville, Québec, Canada, J4B 6Y4

ABSTRACT

Photoacoustic tomography (PAT) and ultrasonography (US) of biological tissues usually rely on ultrasonic transducers for the detection of ultrasound. For an optimum sensitivity, transducers require a physical contact with the tissue using a coupling fluid (water or gel). Such a contact is a major drawback in important potential applications such as surgical procedures on human beings and small animal imaging in research laboratories. On the other hand, laser ultrasonics (LU) is a well established optical technique for the non-contact generation and detection of ultrasound in industrial materials. In this paper, the remote optical detection scheme used in industrial LU is adapted to allow the detection of ultrasound in biological tissues while remaining below laser exposure safety limits. Both non-contact PAT (NCPAT) and non-contact US (NCUS) are considered experimentally using a high-power single-frequency detection laser emitting suitably shaped pulses and a confocal Fabry-Perot interferometer in differential configuration. It is shown that an acceptable sensitivity is obtained while remaining below the maximum permissible exposure (MPE) of biological tissues. Results were obtained *ex vivo* on chicken breast specimens with embedded inclusions simulating blood vessels optical properties. Sub-mm inclusions are readily detected at depths approaching 1 cm. The method is expected to be applicable to living tissues.

Keywords: biomedical imaging, photoacoustic tomography, ultrasonography, laser ultrasonics, laser safety limits, tissue imaging, chicken breast

1. INTRODUCTION

Biomedical imaging techniques are presently intensively developed [1]. Photoacoustic tomography (PAT), which provides images of the optical absorption contrast, holds promise for many biomedical applications [2,3]. Ultrasonography (US) is a well established imaging modality providing acoustic properties of tissues. Both PAT and US usually rely on ultrasonic transducers in contact with the tissue using a coupling fluid (water or gel). Unfortunately, a physical contact is not suitable for many applications [4]. For example, during brain surgery, the transducer array must be inserted in a sterile sleeve and the sterile saline solution used as coupling medium requires a horizontal working plane. Most extracorporeal applications can use coupling fluids but some, such as burn diagnostic, cannot. Applications related to ophthalmology may also benefit from a non-contact detection of acoustic signals [5]. For small animal imaging, immersion in water significantly complicates the procedure [6]. Consequently, non-contact optical detection of ultrasound in biological tissues is of great interest. Moreover, generation and detection of ultrasound by remote optical means would facilitate endoscopic implementations of PAT and US as well as compatibility with other imaging modalities such as optical coherence tomography (OCT) [2,5,7]. Air-coupled transducers [8] have been considered for PAT but their limited sensitivity could be difficult to overcome, especially when spatial resolution is needed. Attempts have been made to replace piezoelectric transducers by optical means but most of these attempts require a contact with the tissue [9-12].

Laser ultrasonics (LU) is a well established optical technique allowing non-contact generation and detection of ultrasound [13]. LU is mostly applied to industrial materials such as metals, plastics and polymer-matrix composites. Ultrasound is laser generated by thermoelastic expansion or by slight ablation at the surface of the material and acoustic reflections coming back to the surface are detected using a laser beam reflected/backscattered by the material. The reflected/backscattered light, which is phase modulated by the surface displacement, is demodulated with a large

* guy.rousseau@cnrc-nrc.gc.ca

throughput interferometer such as a confocal Fabry-Perot interferometer (CFPI) [14,15] or a photorefractive interferometer [16,17]. High sensitivity is obtained by using a high power detection laser and operating in a shot-noise-limited detection regime. The challenge in applying the optical detection scheme used in LU to biomedical imaging consists in obtaining an acceptable sensitivity without exceeding laser exposure safety limits [18]. Non-contact PAT has been recently demonstrated on materials [19] but, to our knowledge, not on biological tissues for which the optical properties can differ significantly and laser safety limits cannot be ignored.

In this work, the optical detection scheme used in industrial LU is adapted to the safe detection of ultrasound in biological tissues. The technique does not require any contact, coupling medium or surface preparation. Non-contact PAT and US (NCPAT and NCUS) are implemented using a single apparatus, the difference between both imaging modes being found in the reconstruction algorithms. This first demonstration is based on three strategies. First, a safe level of laser radiation is achieved by shortening high-energy detection laser pulses to the propagation time of ultrasound. Second, quantum-limited sensitivity is reached using an optical phase demodulator in differential configuration. Third, nearly diffraction-limited images are obtained by sensing remotely the surface profile of the tissue. Those strategies allow a safe detection of inclusions exhibiting optical and acoustic contrasts. Inclusions down to 0.5 mm in size located at depths approaching 1 cm were detected *ex vivo* in chicken breast specimens. The technique is expected to be applicable *in vivo* on beating/moving internal organs or skin.

2. EXPERIMENTAL SETUP

2.1 Laser sources

Using laser beams to generate and detect ultrasound in biological tissues immediately leads to opposite requirements. First, the sensitivity of the measurement can only be increased by using a higher power of laser radiation. Second, the laser power is limited by safety limits, namely, the maximum permissible exposure (MPE), to avoid damaging the biological tissue [18]. Those opposite requirements necessitate an appropriate laser exposure management.

Efficient laser generation of acoustic waves is obtained with sufficiently short laser pulses compared to thermal and stress relaxation times [1]. Typically, few nanosecond pulses produced by Q-switched lasers are appropriate. In practice, the tissue must be exposed on a large surface area to obtain a uniform illumination inside the tissue and the generation laser pulse energy is limited by the MPE for a repetitive exposure [18]. In the absence of free parameters for the generation laser, the laser exposure management is thus related to the detection laser.

When probing soft tissues at depths limited to 1 or 2 cm, the maximum propagation delay of ultrasonic waves is about 25 µs since the propagation velocity is about 1.5 mm/µs in soft tissues. In order to minimize laser exposure, the detection laser illumination should be limited to the ultrasound propagation delay. For most industrial applications, a master oscillator power amplifier (MOPA) emitting powerful long pulses is appropriate. Such a laser source can be adapted to biomedical applications by limiting the pulse duration without losing energy in the laser system. This is done by adding an intensity modulator (IMOD) between the single-frequency continuous wave (cw) master oscillator and the following pulsed power amplifier. A schematic diagram of such a laser source is shown in Fig. 1a.

The IMOD allows inhibiting the amplifier output at the beginning of each pumping flash by setting its transmission to zero. The energy then builds up in the amplifier laser rods (LRs). Before the end of each pumping flash, the transmission of the IMOD is increased gradually to release the stored energy and obtain the desired pulse duration and shape at the amplifier output. Without pulse shaping (Fig. 1b), the output pulses at the exit of the pulsed power amplifier have an energy of 35 mJ, a peak power of 280 W and a duration of 110 µs (FWHM: full width at half maximum). With pulse shaping (Fig. 1c), the output pulses tailored for this experiment have an energy of 14 mJ, a peak power of 560 W and a duration of 24 µs (FWHM). Reducing the pulse duration thus increases the available peak power. More importantly, the peak power for a given energy is about 5 times higher with the tailored pulses. We have chosen using a tailored pulse shape with an increasing instantaneous power for two reasons. First, this eliminates strong signal oscillations at the output of high-pass filters preceding signal digitization. Second, the sensitivity increases with time to facilitate the detection of weaker signals arriving at larger time delays (coming from larger depths in the tissue).

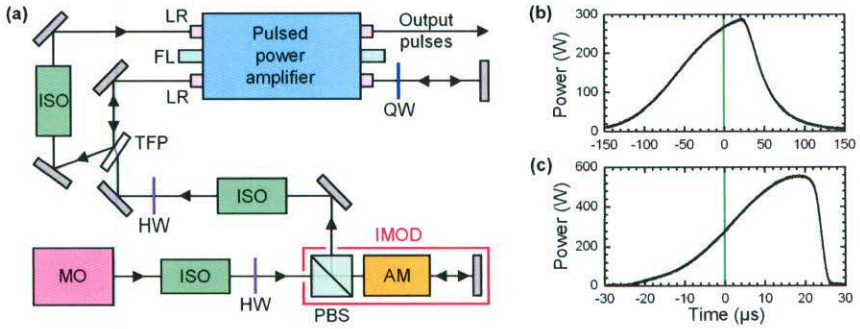

Fig. 1 (a) Layout of the detection laser. MO, Nd:YAG cw master oscillator; ISO, optical isolator; HW, half-wave plate; PBS, polarizing beam splitter; AM, amplitude modulator; IMOD, intensity modulator; TFP, thin-film polarizer; LR, Nd:YAG laser rod; FL, flashlamp; QW, quarter-wave plate. Other components are plane dielectric mirrors. (b) Pulse shape at the output of the detection laser without pulse shaping. (c) Pulse shape tailored for the experiment using the IMOD. The generation laser pulse occurs at t = 0 µs (green lines in b and c).

2.2 Scanning and detection systems

A schematic diagram of the scanning setup is shown in Fig. 2a. The generation laser (not shown) is a Q-switched laser emitting 5 ns pulses at 532 nm with a repetition frequency of 10 Hz. The generation laser beam (shown in green) is directed toward the biological tissue specimen after beam expansion and transmission through a line mask blocking the generation laser on the detection scan line. The purpose of the line mask was to eliminate any overlap between the detection and generation laser illumination during the entire scan to increase the allowed laser power (see also Subsection 3.2). This allows using the single shot safety limit for the detection laser and the repetitive exposure safety limit for the generation laser. The detection laser beam (shown in red) is transmitted to the setup with a multimode optical fiber. A sample of the detection laser beam is first deflected by a beam splitter (BS) and coupled into an optical fiber as a reference beam for phase noise elimination. The detection laser beam is then focused on a 400 µm diameter spot on the tissue specimen. A small prism mirror (P) in front of the collecting optics is used to direct the detection laser beam to the tissue without coupling stray light into the collecting optics. The resulting illumination/detection geometry is shown in the inset (Fig. 2a) where the elliptic green area is the generation laser spot (masked on the scan line) and the red area is the detection laser spot. The collecting optical system uses two lenses assemblies (LAs) with focal lengths of 33 mm for collimating and coupling the reflected/backscattered light (shown in yellow) into the optical fiber (400 µm core diameter, 0.39 numerical aperture) carrying the signal beam. The biological tissue specimen is located on a computer-controlled motorized stage allowing displacements along the scanning axis x and the focusing axis z. The working distance between the biological tissue and the collecting optics was about 25 mm.

The phase demodulation of the collected light is done with an actively stabilized CFPI mounted in differential configuration to achieve both intensity and phase noise reduction (Fig. 2b) [20]. The horizontal polarization is used to analyze light from the tissue specimen (signal beam) and the vertical polarization is used to measure the phase noise of the detection laser (reference beam). The CFPI is a 1 m long cavity with mirrors' reflectivity of 94.5%. The back mirror is mounted on a piezoelectrically actuated mount (PZM) fed by a 10 Hz servo loop ensuring stabilization at half-maximum of the carrier frequency transmission. The optical system inertia ensures a good stability within each measurement time window of about 20 µs. Such a CFPI is thus already compatible with *in-vivo* measurements. The demodulation response of the CFPI presents a peak demodulation response around 2 MHz and remains significant between 400 kHz and 9 MHz. For both reference and signal beams, a differential detector (DD) was used to remove intensity noise (Fig. 2b). Each DD uses two InGaAs photodiodes in series DC-coupled to a transimpedance amplifier followed by a high-pass filter (300 kHz cutoff frequency) and a voltage amplifier. Phase noise of the detection laser was eliminated by the active filtering explained as follows. First, the amplitude of the signal channel before the generation laser pulse was multiplied to obtain an rms noise equal to that of the reference channel in the same time window. Then, iterations around this first value have allowed determining the optimum amplitude multiplication factor to minimize the residual noise on the difference between both channels. Typically, the residual noise was comparable to the shot noise level calculated from nominal values of the transimpedance gain and InGaAs photodiodes' quantum efficiency. The spectrum of the residual noise was practically white in the frequency range kept for the analysis (0.5 to 3 MHz).

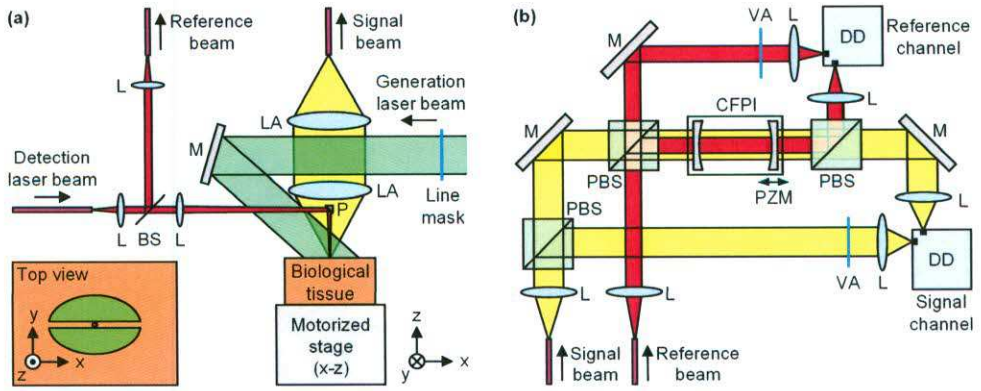

Fig. 2 (a) Schematic diagram of the biological tissue scanning setup: LA, lenses assembly; L, lens; M, plane mirror; BS, beam splitter; P, gold coated hypotenuse prism. (b) Schematic diagram of the CFPI in differential configuration: PBS, polarizing beam splitter; PZM, piezoelectrically actuated mirror mount; VA, variable attenuator; DD, differential detector.

2.3 Remote surface profilometer

The surface profile was measured prior to each scan using a slight modification of the scanning setup (Fig. 2a). A mechanical optical beam chopper was temporarily inserted between the signal beam optical fiber and the adjacent lenses assembly. A 5 mW green laser pointer was injected into the other end of the signal beam optical fiber. The laser beam backscattered by the tissue was collected back into the signal beam optical fiber and detected with an amplified Si photodiode followed by a lock-in amplifier. For each lateral position x, the vertical position z was scanned (100 µm step size) over about 3 mm and the position of the maximum signal after a Gaussian fit with the z-scan intensity profile provided the position of the surface with an uncertainty of about 100 µm.

3. METHODOLOGY

3.1 Image reconstruction

A typical image is obtained from 60 to 80 A-scans, each measured with a single detection laser pulse (no averaging). All A-scans are grouped in a raw B-scan image which is processed with the synthetic aperture focusing technique (SAFT) [21]. The SAFT algorithm was applied in the time domain and modified to take into account the surface profile of the biological tissue. When measuring remotely on curved surfaces with non negligible height variations compared to the minimum ultrasonic wavelength (about 0.5 mm at 3 MHz), the surface profile is an essential input for a reliable image reconstruction. In our experiment, the surface profile was measured prior to the scan (Subsection 2.3). Each raw B-scan image, once linked with the surface profile, contains the necessary information for both NCPAT and NCUS reconstructions; the only difference being related to the expression of the propagation delay.

In the case of NCPAT, the optically scattering tissue is considered to have a low background absorption at the generation laser wavelength, except for optically absorbing inclusions such as blood vessels. In this case, the thermoelastic generation occurs on each inclusion with a strength related to the product of the local laser fluence and the absorption coefficient of the inclusion. Ultrasonic waves then propagate up to the surface were they can be detected.

In the case of NCUS, the combination of the weak endogenous optical absorption at the generation laser wavelength with the high generation laser light fluence at the surface of the biological tissue (or close to it) is considered to be sufficiently large to produce an acoustic wave by thermoelastic generation. The unprepared surface of the tissue is thus the source of a probing ultrasonic wave which has an initial wavefront following the surface topography. Ultrasonic reflections produced by inclusions exhibiting an acoustic impedance mismatch with the surrounding tissue go back to the surface were they can be detected. Consequently, the technique is intrinsically bimodal; the same data being used for both processed images. The only difference is the temporal delay used for the image reconstruction: the one-way propagation delay is used for NCPAT and the two-way propagation delay is used for NCUS.

After applying the active filter (Subsection 2.2), each A-scan was numerically filtered with a third order Bessel-type bandpass filter using typical cutoff frequencies of 0.5 and 3 MHz. With a lateral step size of 400 μm, using frequencies higher than 3 MHz only increases the background noise without a significant gain in spatial resolution [22]. Each A-scan was delayed according to the measured surface profile and to the speed of sound in the specimen. The reconstruction grid included interpolation along the axis x to reduce the lateral pixel size to 100 μm instead of the experimental lateral step of 400 μm. The vertical size of the pixel was also set to 100 μm. Consequently, all images were obtained with a pixel size of 100×100 μm^2. For both imaging modes, the time derivative of each A-scan was used to account for the fact that pressure is proportional to the velocity of the surface, not to displacement [19].

3.2 Laser safety limits

For the generation laser, the average intensity must be considered since there is a significant overlap of the surface illuminated by the generation laser between successive points of the scan. The illuminated elliptic surface of 4.0 cm × 2.5 cm has an area of 7.9 cm^2. With 100 mJ pulses at 10 Hz, this corresponds to an average intensity of 130 mW/cm^2, well below the MPE at 532 nm (200 mW/cm^2) [18]. The single-shot MPE (expressed in terms of fluence) can be used at the detection laser wavelength (1064 nm) since there is no overlap between successive points of the scan. The line mask also eliminates any overlap between the detection laser spots and the area illuminated repetitively by generation laser. Assuming a pulse duration t of about 25 μs, the MPE is given by $C \cdot t^{0.25} = 0.39$ J/cm^2 since C = 5.0 $J/cm^2/s^{0.25}$ at 1064 nm [18]. The 400 μm diameter detection spot corresponds to an area A = 1.3×10^{-3} cm^2. The maximum energy per pulse is thus equal to $E = A \cdot C \cdot t^{0.25} = 0.5$ mJ, which is the pulse energy used in the experiment (after attenuation of the available 14 mJ).

3.3 Tissue specimens and blood vessel phantoms

Chicken breasts purchased in a grocery store were cut parallel to the natural surface to obtain a uniform thickness of about 10 mm. The natural surface of the upper piece was used for laser measurements. In the lower piece of chicken breast, 1 to 3 mm deep incisions were made with a scalpel and gently filled with vegetable oil using a syringe before inserting exogenous inclusions. Vegetable oil was also poured between both pieces of chicken breast for a better ultrasonic contact.

Blood vessels were simulated with polyester thin wall tubes filed with India ink diluted in water to obtain an absorption coefficient μ_a comparable to that of whole blood at 532 nm, which is about 235 cm^{-1} for oxyhemoglobin and 217 cm^{-1} for deoxyhemoglobin. Those values were obtained using a whole blood concentration of hemoglobin of 150 g Hb/liter [23]. The polyester tubes were optically transparent at visible and near infrared wavelengths and the nominal wall thickness was 12.7 μm. The negligible wall thickness compared to the shortest ultrasound wavelength considered in the experiment (about 0.5 mm) also ensured a good acoustic transparency.

4. RESULTS

Experimental results were obtained with a chicken breast specimen including embedded objects. The embedded objects shown in Fig. 3a were chosen to produce different combinations of photoacoustic and ultrasonic responses. Blood vessel phantoms (*i*) and (*iii*) were prepared to mimic the optical blood absorption coefficient at the generation laser wavelength while minimizing the acoustic impedance mismatch with the surrounding tissue (see Subsection 3.3). Metal wires (*ii*) and (*iv*) were used to provide a strong ultrasonic impedance mismatch. One of them (*ii*) was painted in white to minimize the photoacoustic response while the second one (*iv*) was unpainted to provide both a photoacoustic response and an ultrasonic impedance mismatch. All embedded objects were inserted parallel to each other at a depth of about 10 mm and the scan line on the surface of the chicken breast specimen was perpendicular to their common orientation. A photograph of a chicken breast specimen is shown in Fig. 3b: the red arrow represents the 32 mm long scan line whereas all embedded objects are schematically shown over the photograph.

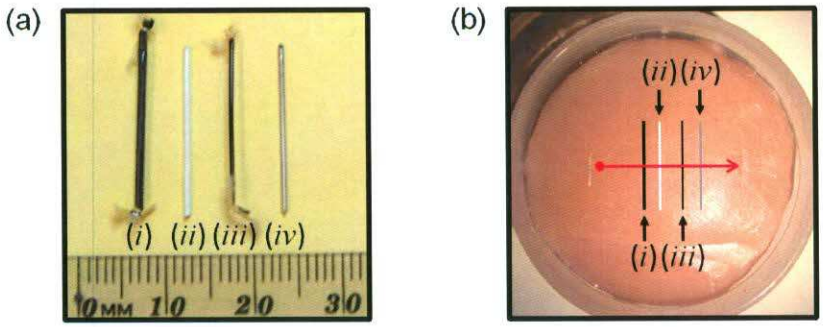

Fig. 3 Photographs of (a) typical embedded objects and (b) a chicken breast specimen.

The raw B-scan image obtained with the objects described previously is shown in Fig. 4a. Although the photoacoustic signals (p_i, p_{iii} and p_{iv}) as well as the ultrasonic reflections (u_{ii} and u_{iv}) can all be seen, the result is somewhat noisy and the signal level at the beginning of the scan is lower due to a higher inclination of the chicken breast specimen (explained below). Figure 4b shows the detection laser phase noise registered simultaneously to the raw B-scan image using the reference beam. Once the active filtering is applied using both the raw B-scan and the phase noise measurement, a clean B-scan image is obtained (Fig. 4c). It is then clearly seen that this B-scan contain the photoacoustic responses of absorbing blood vessel phantoms (p_i, p_{iii}) and the grayish metal wire (p_{iv}) as well as the ultrasonic reflections (u_{ii} and u_{iv}) of both metal wires. As expected, each signal appears as a nearly hyperbolic shape before applying the SAFT algorithm.

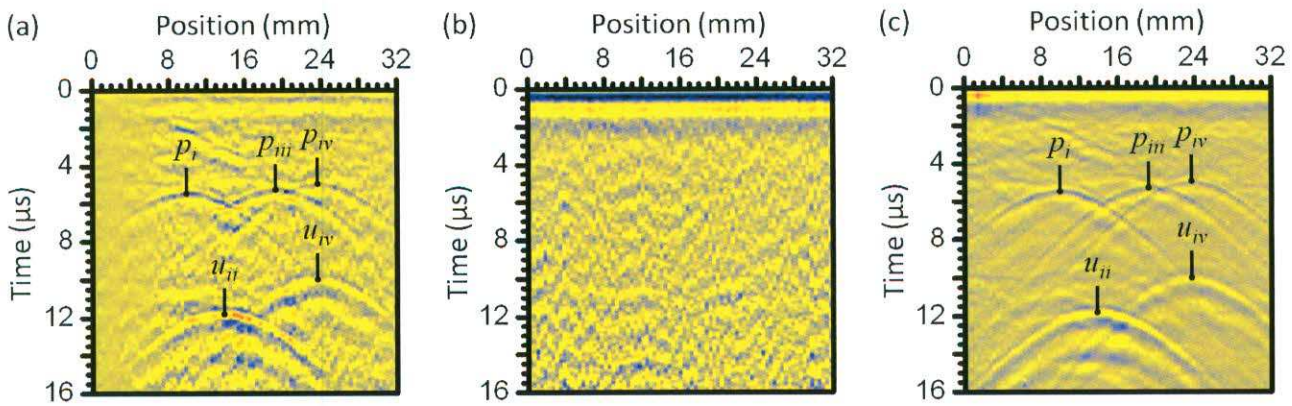

Fig. 4 (a) Raw B-scan image. (b) Phase noise of the detection laser measured simultaneously to the raw B-scan. (c) Clean B-scan image obtained after noise reduction using active filtering.

The clean B-scan image shown in Fig. 4c is then processed with the NCPAT algorithm and the NCUS algorithm. The NCPAT image (Fig. 5a) and the NCUS image (Fig. 5b) of the same chicken breast specimen clearly exhibits the embedded objects highlighted by arrows and zoomed below their respective image. The 1.0 mm diameter and 0.5 mm diameter blood vessel phantoms (respectively, *i* and *iii*) are mainly seen in the NCPAT image. The 0.8 mm diameter white painted metal wire (*ii*) is only seen in the NCUS image and the 0.7 mm diameter grayish metal wire (*iv*) is seen in both NCPAT and NCUS images. This demonstrates the capability of the non-contact approach to discriminate photoacoustic and ultrasonic signatures of each object starting from a single data set. The NCPAT image also exhibits some faint endogenous absorption sites (for example above object *i*). Successive measurements with the same specimen have shown a good repeatability of the resulting NCPAT and NCUS images. Faint photoacoustic artifacts (p_i, p_{iii} and p_{iv}) seen in the upper part of the NCUS image (Fig. 5b) are related to objects (*i*, *iii*, and *iv*) which are not properly focused by the NCUS reconstruction algorithm. These artifacts are a consequence of the bimodal character of the non-contact method and the fact that photoacoustic signals necessarily precede ultrasound signals (for a given object).

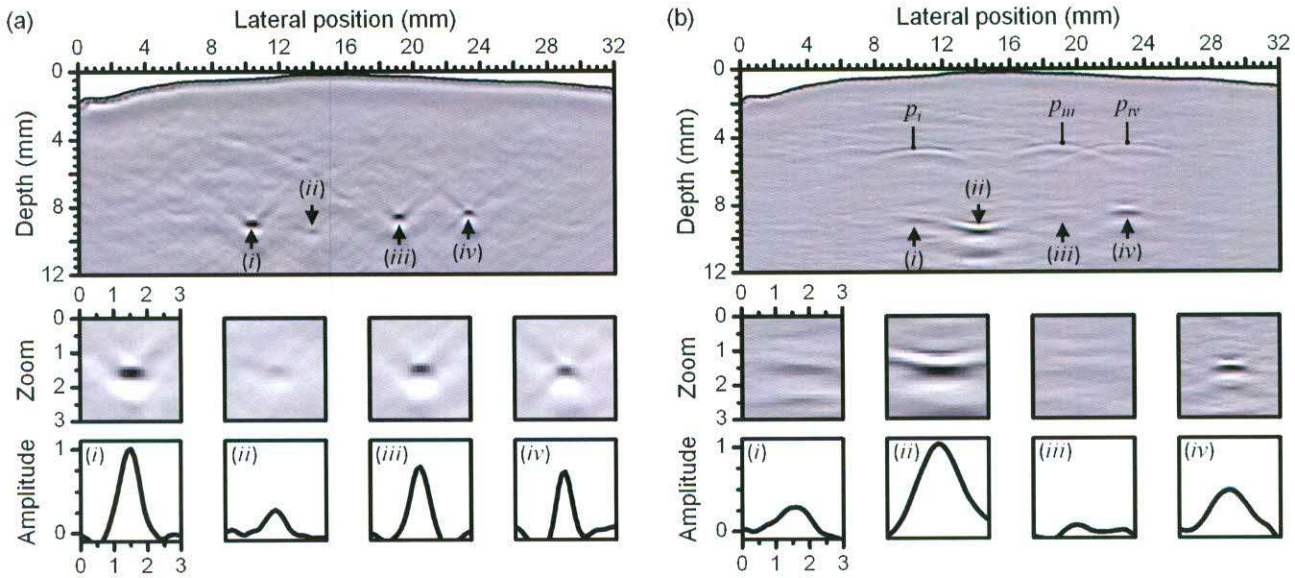

Fig. 5 Images of a chicken breast specimen. (a) NCPAT image obtained with the following embedded objects (respective diameters in parenthesis): *i*, blood vessel phantom (1 mm); *ii*, white painted metal wire (0.8 mm); *iii*, blood vessel phantom (0.5 mm); *iv*, unpainted greyish metal wire (0.7 mm). (b) Corresponding NCUS image. All scales are in mm except for amplitude profiles (in arbitrary units).

5. CONCLUSION

The results presented herein demonstrate that NCPAT and NCUS can be performed *ex vivo* on soft biological tissues. Sub-millimeter endogenous and exogenous inclusions have been detected at depth of about 1 cm. It is clearly shown that the highly scattering surface of a soft tissue provides a sufficiently strong diffused reflectivity to measure the ultrasonic displacement of the surface while remaining below the MPE. This however requires limiting the pulse duration of the detection laser to the propagation time of ultrasound. Using a differential configuration of the CFPI has also been essential to reach a quantum-limited sensitivity by removing both intensity and phase noise of the detection laser. For NCPAT, the 1D surface profile measurement has been sufficient to obtain nearly diffraction-limited images using time-domain SAFT. However, for the NCUS imaging mode, a 2D surface topography measurement and a better modelling of the probing ultrasonic wave would be essential to achieve diffraction-limited images.

REFERENCES

[1] Wang, L. V. and Wu, H., [Biomedical Optics: Principles and Imaging], John Wiley and Sons, Hoboken, New Jersey (2007).

[2] Beard, P., "Biomedical photoacoustic imaging," Interface Focus 1, 602-631 (2011).

[3] Wang, L. V., ed., [Photoacoustic Imaging and Spectroscopy], CRC Press, Boca Raton, Florida (2009).

[4] Ntziachristos, V., Yoo, J. S. and van Dam, G. M., "Current concepts and future perspectives on surgical optical imaging in cancer," J. Biomed. Opt. 15, 066024-1/12 (2010).

[5] Jiao, S., Jiang, M., Hu, J., Fawzi, A., Zhou, Q., Shung, K. K., Puliafito, C. A. and Zhang, H. F., "Photoacoustic ophthalmoscopy for *in vivo* retinal imaging," Opt. Express 18, 3967-3972 (2010).

[6] Wang, X., Pang, Y., Ku, G., Xie, X., Stoica, G., Wang, L. V., "Noninvasive laser-induced photoacoustic tomography for structural and functional *in vivo* imaging of the brain," Nature Biotech. 21, 803-806 (2003).

[7] Zhang, E. Z., Povazay, B., Laufer, J., Alex, A., Hofer, B., Pedley, B., Glittenberg, C., Treeby, B., Cox, B., Beard, P. and Drexler, W., "Multimodal photoacoustic and optical coherence tomography scanner using an all optical detection scheme for 3D morphological skin imaging," Biomed. Opt. Express 2, 2202-2215 (2011).

[8] Kolkman, R. G. M., Blomme, E., Cool, T., Bilcke, M., van Leeuwen, T. G., Steenbergen, W., Grimbergen, K. A., and den Heeten, G. J., "Feasibility of noncontact piezoelectric detection of photoacoustic signals in tissue-mimicking phantoms," J. Biomed. Opt. 15, 055011-1/4 (2010).
[9] Xie, Z., Chen, S., Ling, T., Guo, L. J., Carson, P. L. and Wang, X., "Pure optical photoacoustic microscopy," Opt. Express 19, 9027-9034 (2011).
[10] Nuster, R., Gruen, H., Reitinger, B., Burgholzer, P., Gratt, S., Passler, K. and Paltauf, G., "Downstream Fabry-Perot interferometer for acoustic wave monitoring in photoacoustic tomography," Opt. Lett. 36, 981-983 (2011).
[11] Payne, B. P., Venugopalan, V., Mikić, B. B. and Nishioka, N. S., "Optoacoustic tomography using time-resolved interferometric detection of surface displacement," J. Biomed. Opt. 8, 273-280 (2003).
[12] Wang, Y., Li, C. and Wang, R. K., "Noncontact photoacoustic imaging achieved by using a low-coherence interferometer as the acoustic detector," Opt. Lett. 36, 3975-3977 (2011).
[13] Scruby, C. B. and Drain, L. E., [Laser Ultrasonics: Techniques and Applications], Adam Hilger, Bristol, UK (1990).
[14] Monchalin, J.-P., "Optical detection of ultrasound at a distance using a confocal Fabry-Perot interferometer," Appl. Phys. Lett. 47, 14-16 (1985).
[15] Monchalin, J.-P., "Optical detection of ultrasound," IEEE Trans. Ultrason. Ferroelectr. Freq. Control 33, 485-499 (1986).
[16] Ing, R. K. and Monchalin, J.-P., "Broadband optical detection of ultrasound by two-wave mixing in a photorefractive crystal," Appl. Phys. Lett. 59, 3233-3235 (1991).
[17] Blouin, A. and Monchalin, J.-P., "Detection of ultrasonic motion of a scattering surface by two-wave mixing in a photorefractive GaAs crystal," Appl. Phys. Lett. 65, 932-934 (1994).
[18] American National Standard for the Safe Use of Lasers ANSI Z136.1-2007 (Laser Institute of America, Orlando, Florida, 2007).
[19] Berer, T., Hochreiner, A., Zamiri, S. and Burgholzer, P., "Remote photoacoustic imaging on solid material using a two-wave mixing interferometer," Opt. Lett. 35, 4151-4153 (2010).
[20] Blouin, A., Padioleau, C., Néron, C., Lévesque, D. and Monchalin, J.-P., "Differential confocal Fabry-Perot for the optical detection of ultrasound," in Rev. of Prog. in QNDE 26, D. O. Thompson and D. E. Chimenti, eds. (Plenum, New York, 2007), pp. 193-200.
[21] Davies, J., Simonetti, F., Lowe, M. and Cawley, P., "Review of synthetically focused guided wave imaging techniques with application to defect sizing," in Rev. of Prog. in QNDE 25, D. O. Thompson and D. E. Chimenti, eds. (American Institute of Physics, New York, 2006), pp. 142-149.
[22] Lévesque, D., Blouin, A. and Monchalin, J.-P., "Performance of laser-ultrasonic F-SAFT imaging," Ultrasonics 40, 1057-1063 (2002).
[23] Prahl, S., Oregon Medical Laser Center. http://omlc.ogi.edu/spectra/hemoglobin/index.html.